

expression of Hes1 dramatically reduced *SCO2* and *TIGAR* expression (Figure 6E), which suggests that Notch-Hes1 signaling modulates the metabolic pathway. Intriguingly, our results also indicate that Hes1 could suppress the expression of *TIGAR* and *SCO2*, a p53 target gene. It has been reported that Notch signaling suppresses p53 in lymphomagenesis [47]. Moreover, Kim et al. reported that NICD1 inhibits p53 phosphorylation and represses p53 transactivation by interacting with p53 [48]. In addition, DAPT treatment resulted in the enhancement of p53 activity in the hypoxic conditions (Figure 4H and I). Therefore, it is possible that p53 activation was regulated by Notch signaling in hADMPCs, although we did not observe a decrease in p53 activity in hypoxic conditions in this study (Figure 4). Further analysis will be required to determine whether p53 activity is suppressed in hypoxic conditions over a longer period of culture.

Cells undergoing active proliferation utilize large amounts of glucose through glycolysis, producing pyruvate for use in substrates (amino acids and lipids) and the pentose shunt for use in nucleic acid substrates, and also producing NADPH as a reducing agent to counter oxidative stress [18,56]. In the current study, 5% O<sub>2</sub> actually increased proliferation and decreased the accumulation of ROS, which may be involved in the reduction of senescence (Figure 1). Because accumulation of endogenous ROS might be a major reason for replicative senescence [20], enhancing glycolysis in cultured cells may improve the quality of the cells by suppressing premature senescence. Kondoh *et al.* demonstrated that enhanced glycolysis is involved in cellular immortalization through reduction of intrinsic ROS production [14,18,19]. Therefore, it is possible that the extension of lifespan observed in our experimental conditions was caused by the reduction of intracellular ROS

levels through enhanced glycolysis by Notch signaling. Our data indicate that aerobic glycolysis is utilized for proliferation of hADMPCs because the glycolytic inhibitor 2-DG attenuates the proliferation rate of hADMPCs (Figure 7A). Intriguingly, the aerobic respiration block by  $\text{NaN}_3$  did not decrease the proliferation; rather, it increased proliferation at a low concentration (Figure 7B), which may support our data indicating that the metabolic switch from mitochondrial respiration to glycolysis provides a growth advantage to hADMPCs. However, the question of whether the enhanced glycolysis really contributes to the prolonged lifespan in hADMPCs remains to be determined in this study.

In the current study, the molecular mechanism for how Notch signaling is activated in 5%  $\text{O}_2$  conditions was explored. It has been reported that Notch1 activity is influenced by oxygen concentration [41,42,57]. In melanoma cells, hypoxia (2%  $\text{O}_2$ ) resulted in increased expression of Notch1 by HIF-1 $\alpha$  and also by Akt through NF- $\kappa$ B activity [42]. Similarly, in hypoxic breast cancer cells, Notch ligand JAG2 was shown to be transcriptionally activated by hypoxia (1%  $\text{O}_2$ ) in a HIF-1 $\alpha$  dependent manner, resulting an elevation of Notch signaling [41]. In contrast, in hESCs continuously cultured in 5%  $\text{O}_2$ , alteration of the Notch pathway seems to be independent of HIF-1 $\alpha$  [57]. In our system, Notch1 activation was not likely dependent on HIF-1 $\alpha$  and HIF-2 $\alpha$  because these proteins did not accumulate in the Hx condition. In contrast, our results indicate that the 5%  $\text{O}_2$  condition activated Akt and NF- $\kappa$ B signaling (Figure 4), which suggests that these molecules may activate Notch signaling in hADMPCs. NF- $\kappa$ B was previously shown to increase Notch1 activity indirectly by increasing the expression of Notch ligand Jagged1 in HeLa, lymphoma, and myeloma cells [58]. In addition, Akt regulated

Notch1 by increasing Notch1 transcription through the activity of NF- $\kappa$ B in melanoma cells [42]. Further analysis is required to clarify the mechanism underlying this phenomenon.

In conclusion, the 5% oxygen condition conferred a growth advantage through a metabolic shift to glycolysis, improved the proliferation efficiency, prevented the cellular senescence, and maintained the undifferentiated status of hADMPCs. These observations thus provide new regulatory mechanisms for the maintenance of stemness observed in 5% oxygen conditions. In addition, our study sheds new light on the regulation of replicative senescence, which might have impact for quality control of hADMPC preparations used for therapeutic applications.

### **Acknowledgments**

The authors would like to thank Koichi Sakaguchi, Mio Oishi, Mika Uemura, and Kei Sawaragi for technical support. This work was supported by MEXT KAKENHI Grant Number 24791927 to H.M. This work was also supported in part by grants from the Ministry of Health, Labor, and Welfare of Japan and a grant from the Program for Promotion of Fundamental Studies in Health Sciences of the National Institute of Biomedical Innovation (NIBIO).

### **Disclosure Statement**

The authors declare no conflict of interest. No competing financial interests exist.

## References

1. Okura H, H Komoda, A Saga, A Kakuta-Yamamoto, Y Hamada, Y Fumimoto, CM Lee, A Ichinose, Y Sawa and A Matsuyama. (2010). Properties of hepatocyte-like cell clusters from human adipose tissue-derived mesenchymal stem cells. *Tissue engineering. Part C, Methods* 16:761-70.
2. Okura H, A Matsuyama, CM Lee, A Saga, A Kakuta-Yamamoto, A Nagao, N Sougawa, N Sekiya, K Takekita, Y Shudo, S Miyagawa, H Komoda, T Okano and Y Sawa. (2010). Cardiomyoblast-like cells differentiated from human adipose tissue-derived mesenchymal stem cells improve left ventricular dysfunction and survival in a rat myocardial infarction model. *Tissue engineering. Part C, Methods* 16:417-25.
3. Okura H, H Komoda, Y Fumimoto, CM Lee, T Nishida, Y Sawa and A Matsuyama. (2009). Transdifferentiation of human adipose tissue-derived stromal cells into insulin-producing clusters. *Journal of artificial organs : the official journal of the Japanese Society for Artificial Organs* 12:123-30.
4. Safford KM, SD Safford, JM Gimble, AK Shetty and HE Rice. (2004). Characterization of neuronal/glia differentiation of murine adipose-derived adult stromal cells. *Experimental neurology* 187:319-28.
5. Leu S, YC Lin, CM Yuen, CH Yen, YH Kao, CK Sun and HK Yip. (2010). Adipose-derived mesenchymal stem cells markedly attenuate brain infarct size and improve neurological function in rats. *Journal of translational medicine* 8:63.
6. Ikegame Y, K Yamashita, S Hayashi, H Mizuno, M Tawada, F You, K Yamada, Y Tanaka, Y Egashira, S Nakashima, S Yoshimura and T Iwama. (2011). Comparison of mesenchymal stem cells from adipose tissue and bone marrow for ischemic stroke therapy. *Cytotherapy* 13:675-85.
7. Tan B, Z Luan, X Wei, Y He, G Wei, BH Johnstone, M Farlow and Y Du. (2011). AMP-activated kinase mediates adipose stem cell-stimulated neuritogenesis of PC12 cells. *Neuroscience* 181:40-7.
8. Reid AJ, M Sun, M Wiberg, S Downes, G Terenghi and PJ Kingham. (2011). Nerve repair with adipose-derived stem cells protects dorsal root ganglia neurons from apoptosis. *Neuroscience*.
9. Rehman J, D Traktuev, J Li, S Merfeld-Clauss, CJ Temm-Grove, JE Bovenkerk, CL Pell, BH Johnstone, RV Considine and KL March. (2004). Secretion of angiogenic and antiapoptotic factors by human adipose stromal cells. *Circulation* 109:1292-8.
10. Lee EY, Y Xia, WS Kim, MH Kim, TH Kim, KJ Kim, BS Park and JH Sung. (2009). Hypoxia-enhanced wound-healing function of adipose-derived stem cells: increase in stem cell proliferation and

- up-regulation of VEGF and bFGF. Wound repair and regeneration : official publication of the Wound Healing Society [and] the European Tissue Repair Society 17:540-7.
11. Moriyama M, H Moriyama, A Ueda, Y Nishibata, H Okura, A Ichinose, A Matsuyama and T Hayakawa. (2012). Human adipose tissue-derived multilineage progenitor cells exposed to oxidative stress induce neurite outgrowth in PC12 cells through p38 MAPK signaling. *BMC Cell Biol* 13:21.
  12. Wu H, Z Ye and RI Mahato. (2011). Genetically modified mesenchymal stem cells for improved islet transplantation. *Mol Pharm* 8:1458-70.
  13. Wagner W, P Horn, M Castoldi, A Diehlmann, S Bork, R Saffrich, V Benes, J Blake, S Pfister, V Eckstein and AD Ho. (2008). Replicative senescence of mesenchymal stem cells: a continuous and organized process. *PLoS One* 3:e2213.
  14. Kondoh H, ME Lleonart, Y Nakashima, M Yokode, M Tanaka, D Bernard, J Gil and D Beach. (2007). A high glycolytic flux supports the proliferative potential of murine embryonic stem cells. *Antioxid Redox Signal* 9:293-9.
  15. Prigione A, B Fauler, R Lurz, H Lehrach and J Adjaye. (2010). The senescence-related mitochondrial/oxidative stress pathway is repressed in human induced pluripotent stem cells. *Stem Cells* 28:721-33.
  16. Varum S, AS Rodrigues, MB Moura, O Momcilovic, CA Easley, J Ramalho-Santos, B Van Houten and G Schatten. (2011). Energy metabolism in human pluripotent stem cells and their differentiated counterparts. *PLoS One* 6:e20914.
  17. Warburg O, F Wind and E Negelein. (1927). The Metabolism of Tumors in the Body. *J Gen Physiol* 8:519-30.
  18. Kondoh H. (2008). Cellular life span and the Warburg effect. *Exp Cell Res* 314:1923-8.
  19. Kondoh H, ME Lleonart, J Gil, J Wang, P Degan, G Peters, D Martinez, A Carnero and D Beach. (2005). Glycolytic enzymes can modulate cellular life span. *Cancer Res* 65:177-85.
  20. Beckman KB and BN Ames. (1998). The free radical theory of aging matures. *Physiol Rev* 78:547-81.
  21. Ezashi T, P Das and RM Roberts. (2005). Low O<sub>2</sub> tensions and the prevention of differentiation of hES cells. *Proc Natl Acad Sci U S A* 102:4783-8.
  22. Forristal CE, KL Wright, NA Hanley, RO Oreffo and FD Houghton. (2010). Hypoxia inducible factors regulate pluripotency and proliferation in human embryonic stem cells cultured at reduced oxygen tensions. *Reproduction* 139:85-97.
  23. Yoshida Y, K Takahashi, K Okita, T Ichisaka and S Yamanaka. (2009). Hypoxia enhances the generation of induced pluripotent stem cells. *Cell Stem Cell* 5:237-41.
  24. Takubo K, N Goda, W Yamada, H Iriuchishima, E Ikeda, Y Kubota, H Shima, RS Johnson, A Hirao, M Suematsu and T Suda. (2010). Regulation of the HIF-1 $\alpha$  level is essential for hematopoietic stem cells. *Cell Stem Cell* 7:391-402.

25. Santilli G, G Lamorte, L Carlessi, D Ferrari, L Rota Nodari, E Binda, D Delia, AL Vescovi and L De Filippis. (2010). Mild hypoxia enhances proliferation and multipotency of human neural stem cells. *PLoS One* 5:e8575.
26. Tsai CC, YJ Chen, TL Yew, LL Chen, JY Wang, CH Chiu and SC Hung. (2011). Hypoxia inhibits senescence and maintains mesenchymal stem cell properties through down-regulation of E2A-p21 by HIF-TWIST. *Blood* 117:459-69.
27. Takubo K, G Nagamatsu, CI Kobayashi, A Nakamura-Ishizu, H Kobayashi, E Ikeda, N Goda, Y Rahimi, RS Johnson, T Soga, A Hirao, M Suematsu and T Suda. (2013). Regulation of glycolysis by pdk functions as a metabolic checkpoint for cell cycle quiescence in hematopoietic stem cells. *Cell Stem Cell* 12:49-61.
28. Grayson WL, F Zhao, R Izadpanah, B Bunnell and T Ma. (2006). Effects of hypoxia on human mesenchymal stem cell expansion and plasticity in 3D constructs. *J Cell Physiol* 207:331-9.
29. Wang DW, B Fermor, JM Gimble, HA Awad and F Guilak. (2005). Influence of oxygen on the proliferation and metabolism of adipose derived adult stem cells. *J Cell Physiol* 204:184-91.
30. Moriyama M, M Osawa, SS Mak, T Ohtsuka, N Yamamoto, H Han, V Delmas, R Kageyama, F Beermann, L Larue and S Nishikawa. (2006). Notch signaling via Hes1 transcription factor maintains survival of melanoblasts and melanocyte stem cells. *J Cell Biol* 173:333-9.
31. Chiba S. (2006). Notch signaling in stem cell systems. *Stem Cells* 24:2437-47.
32. Moriyama M, H Moriyama, A Ueda, Y Nishibata, H Okura, A Ichinose, A Matsuyama and T Hayakawa. (2012). Human adipose tissue-derived multilineage progenitor cells exposed to oxidative stress induce neurite outgrowth in PC12 cells through p38 MAPK signaling. *BMC Cell Biol* 13:21.
33. Okura H, A Saga, Y Fumimoto, M Soeda, M Moriyama, H Moriyama, K Nagai, CM Lee, S Yamashita, A Ichinose, T Hayakawa and A Matsuyama. (2011). Transplantation of human adipose tissue-derived multilineage progenitor cells reduces serum cholesterol in hyperlipidemic Watanabe rabbits. *Tissue Eng Part C Methods* 17:145-54.
34. Saga A, H Okura, M Soeda, J Tani, Y Fumimoto, H Komoda, M Moriyama, H Moriyama, S Yamashita, A Ichinose, T Daimon, T Hayakawa and A Matsuyama. (2011). HMG-CoA reductase inhibitor augments the serum total cholesterol-lowering effect of human adipose tissue-derived multilineage progenitor cells in hyperlipidemic homozygous Watanabe rabbits. *Biochem Biophys Res Commun* 412:50-4.
35. Moriyama H, M Moriyama, K Sawaragi, H Okura, A Ichinose, A Matsuyama and T Hayakawa. (2013). Tightly regulated and homogeneous transgene expression in human adipose-derived mesenchymal stem cells by lentivirus with tet-off system. *PLoS One* 8:e66274.
36. Sekiya I, BL Larson, JR Smith, R Pochampally, JG Cui and DJ Prockop. (2002). Expansion of human adult stem cells from bone marrow stroma: conditions that maximize the yields of early progenitors and evaluate their quality. *Stem Cells* 20:530-41.
37. Wagner W, F Wein, A Seckinger, M Frankhauser, U Wirkner, U Krause, J Blake, C Schwager, V Eckstein, W Ansorge and AD Ho. (2005). Comparative characteristics of mesenchymal stem cells from human bone marrow, adipose tissue, and umbilical cord blood. *Exp Hematol* 33:1402-16.

38. Hass R, C Kasper, S Bohm and R Jacobs. (2011). Different populations and sources of human mesenchymal stem cells (MSC): A comparison of adult and neonatal tissue-derived MSC. *Cell Commun Signal* 9:12.
39. Gustafsson MV, X Zheng, T Pereira, K Gradin, S Jin, J Lundkvist, JL Ruas, L Poellinger, U Lendahl and M Bondesson. (2005). Hypoxia requires notch signaling to maintain the undifferentiated cell state. *Dev Cell* 9:617-28.
40. Zheng X, S Linke, JM Dias, X Zheng, K Gradin, TP Wallis, BR Hamilton, M Gustafsson, JL Ruas, S Wilkins, RL Bilton, K Brismar, ML Whitelaw, T Pereira, JJ Gorman, J Ericson, DJ Peet, U Lendahl and L Poellinger. (2008). Interaction with factor inhibiting HIF-1 defines an additional mode of cross-coupling between the Notch and hypoxia signaling pathways. *Proc Natl Acad Sci U S A* 105:3368-73.
41. Pietras A, K von Stedingk, D Lindgren, S Pahlman and H Axelson. (2011). JAG2 induction in hypoxic tumor cells alters Notch signaling and enhances endothelial cell tube formation. *Mol Cancer Res* 9:626-36.
42. Bedogni B, JA Warneke, BJ Nickoloff, AJ Giaccia and MB Powell. (2008). Notch1 is an effector of Akt and hypoxia in melanoma development. *J Clin Invest* 118:3660-70.
43. Beitner-Johnson D, RT Rust, TC Hsieh and DE Millhorn. (2001). Hypoxia activates Akt and induces phosphorylation of GSK-3 in PC12 cells. *Cell Signal* 13:23-7.
44. Culver C, A Sundqvist, S Mudie, A Melvin, D Xirodimas and S Rocha. (2010). Mechanism of hypoxia-induced NF-kappaB. *Mol Cell Biol* 30:4901-21.
45. Rohwer N, C Dame, A Haugstetter, B Wiedenmann, K Detjen, CA Schmitt and T Cramer. (2010). Hypoxia-inducible factor 1alpha determines gastric cancer chemosensitivity via modulation of p53 and NF-kappaB. *PLoS One* 5:e12038.
46. Espinosa L, S Cathelin, T D'Altri, T Trimarchi, A Statnikov, J Guiu, V Rodilla, J Ingles-Esteve, J Nomdedeu, B Bellosillo, C Besses, O Abdel-Wahab, N Kucine, SC Sun, G Song, CC Mullighan, RL Levine, K Rajewsky, I Aifantis and A Bigas. (2010). The Notch/Hes1 pathway sustains NF-kappaB activation through CYLD repression in T cell leukemia. *Cancer Cell* 18:268-81.
47. Beverly LJ, DW Felsher and AJ Capobianco. (2005). Suppression of p53 by Notch in lymphomagenesis: implications for initiation and regression. *Cancer Res* 65:7159-68.
48. Kim SB, GW Chae, J Lee, J Park, H Tak, JH Chung, TG Park, JK Ahn and CO Joe. (2007). Activated Notch1 interacts with p53 to inhibit its phosphorylation and transactivation. *Cell Death Differ* 14:982-91.
49. Landor SK, AP Mutvei, V Mamaeva, S Jin, M Busk, R Borra, TJ Gronroos, P Kronqvist, U Lendahl and CM Sahlgren. (2011). Hypo- and hyperactivated Notch signaling induce a glycolytic switch through distinct mechanisms. *Proc Natl Acad Sci U S A* 108:18814-9.
50. Ciofani M and JC Zuniga-Pflucker. (2005). Notch promotes survival of pre-T cells at the beta-selection checkpoint by regulating cellular metabolism. *Nat Immunol* 6:881-8.
51. Welford SM, B Bedogni, K Gradin, L Poellinger, M Broome Powell and AJ Giaccia. (2006). HIF1alpha delays premature senescence through the activation of MIF. *Genes Dev* 20:3366-71.

52. Zhou D, J Xue, JC Lai, NJ Schork, KP White and GG Haddad. (2008). Mechanisms underlying hypoxia tolerance in *Drosophila melanogaster*: hairy as a metabolic switch. *PLoS Genet* 4:e1000221.
53. Funes JM, M Quintero, S Henderson, D Martinez, U Qureshi, C Westwood, MO Clements, D Bourboulia, RB Pedley, S Moncada and C Boshoff. (2007). Transformation of human mesenchymal stem cells increases their dependency on oxidative phosphorylation for energy production. *Proc Natl Acad Sci U S A* 104:6223-8.
54. Kawauchi K, K Araki, K Tobiume and N Tanaka. (2008). p53 regulates glucose metabolism through an IKK-NF-kappaB pathway and inhibits cell transformation. *Nat Cell Biol* 10:611-8.
55. Carter KL, E Cahir-McFarland and E Kieff. (2002). Epstein-barr virus-induced changes in B-lymphocyte gene expression. *J Virol* 76:10427-36.
56. Ak P and AJ Levine. (2010). p53 and NF-kappaB: different strategies for responding to stress lead to a functional antagonism. *FASEB J* 24:3643-52.
57. Prasad SM, M Czepiel, C Cetinkaya, K Smigielska, SC Weli, H Lysdahl, A Gabrielsen, K Petersen, N Ehlers, T Fink, SL Minger and V Zachar. (2009). Continuous hypoxic culturing maintains activation of Notch and allows long-term propagation of human embryonic stem cells without spontaneous differentiation. *Cell Prolif* 42:63-74.
58. Bash J, WX Zong, S Banga, A Rivera, DW Ballard, Y Ron and C Gelinis. (1999). Rel/NF-kappaB can trigger the Notch signaling pathway by inducing the expression of Jagged1, a ligand for Notch receptors. *EMBO J* 18:2803-11.



## Figure legends

**Figure 1. Hypoxia increases proliferation capacity and decreases senescence in hADMPCs.** (A) Growth profiles of hADMPCs under normoxic (red square) and hypoxic (blue square) conditions. The population doubling level (PDL) was determined to be 0 when cells were isolated from human adipose tissue. Cells were maintained until they reached PDL13–15 (passage 3) and then split into four aliquots of equal cell densities. PDL was calculated based on the total cell number at each passage. (B) Detection of normoxic (Nx) and hypoxic (Hx) cells by flow cytometry following incorporation of EdU. (C) Percentages of apoptotic cells with sub-G1 DNA under Nx and Hx conditions. The results are presented as the mean of 3 independent experiments. (D) hADMPCs cultured under Nx and Hx conditions were harvested by trypsin-EDTA and then imaged using a phase-contrast microscope. Arrowheads indicate cells with a larger and more irregular shape. (E) Cells expanded under Nx and Hx conditions were stained with SA- $\beta$ -gal. (F) Cellular ROS detection by the oxidative stress indicator CM-H2DCFDA in hADMPCs under Nx or Hx. Data are presented as the mean fluorescence intensity of 3 independent experiments. Error bars indicate SD. \*P < 0.05 and \*\*P < 0.01 indicate significant difference (independent *t*-test) between Nx and Hx. Scale bars; 100  $\mu$ m.

**Figure 2. Hypoxic culture maintains mesenchymal stem cell properties.** hADMPCs cultured under normoxia (20% O<sub>2</sub>) or hypoxia (5% O<sub>2</sub>) were labeled with antibodies against the indicated antigens and analyzed by flow cytometry. Representative histograms are shown. The respective isotype control is shown as a gray line.

**Figure 3. Hypoxic culture enhances stem cell properties.** hADMPCs were expanded under normoxic and hypoxic conditions. **(A)** Normoxic (20% O<sub>2</sub>) and hypoxic (5% O<sub>2</sub>) cells at passage 8 were induced for 3 weeks to differentiate into osteoblasts and adipocytes and stained with alizarin red and Oil-red O, respectively. The stained dye was extracted and OD values were measured and plotted as the means of 3 independent experiments ± SD. \*P < 0.05. Scale bars, 200 μm. **(B)** Normoxic (20% O<sub>2</sub>) and hypoxic (5% O<sub>2</sub>) cells at passage 8 were induced for 3 weeks to differentiate to chondrocytes, and immunofluorescent analysis of collagen II (red) and Alcian blue staining were performed. The blue signals indicate nuclear staining. Scale bars, 100 μm. Non-induced control cultures in growth medium without adipogenic, osteogenic or chondrogenic differentiation stimuli are shown (Undifferentiated).

**Figure 4. Hypoxic culture condition activates Notch signaling but not HIF proteins.** hADMPCs were expanded under normoxic (20% O<sub>2</sub>) and hypoxic (5% O<sub>2</sub>) conditions. DAPT (1 μM) was added to inhibit Notch signaling. **(A)** Western blot analysis of intracellular domain of Notch1 (Notch1 ICD) expression. Actin served as the loading control. Numbers below blots indicate relative band intensities as determined by ImageJ software. **(B)** Q-PCR analysis of *HES1*. Each expression value was calculated with the  $\Delta\Delta C_t$  method using *UBE2D2* as an internal control. **(C)** Western blot analysis of HES1 in nuclear fractions of hADMPCs. Lamin A/C served as the loading control. **(D, E)** Western blot analysis of HIF-1 $\alpha$  **(D)** and HIF-2 $\alpha$  **(E)**. Cobalt chloride (CoCl<sub>2</sub>) was added at a concentration of 100 μM to stabilize HIF proteins (positive control). **(F)** Western blot analysis of phosphorylated

Akt (p-Akt) and Akt. Actin served as the loading control. Numbers below blots indicate relative band intensities as determined by ImageJ software. **(G)** Western blot analysis of nuclear localization of p65. Lamin A/C served as the loading control. Numbers below blots indicate relative band intensities as determined by ImageJ software. **(H)** Western blot analysis of phosphorylated p53 (p-p53) and p53. Actin served as the loading control. **(I)** Activity of p53 was measured by the p53-luciferase reporter assay. Relative luciferase activity was determined from 3 independent experiments and normalized to pGL4.74 activity.

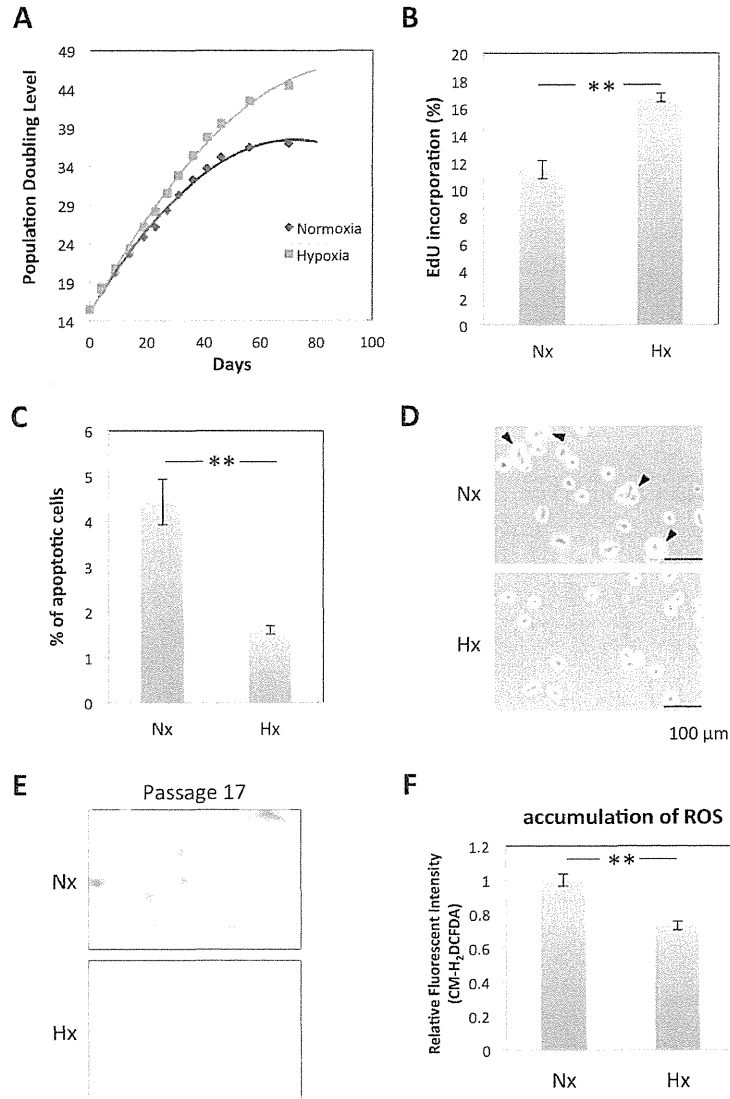
**Figure 5. Notch signaling is indispensable for acquisition of the advantageous properties of hADMPCs.**

hADMPCs were expanded under normoxic (20% O<sub>2</sub>; Nx) and hypoxic (5% O<sub>2</sub>; Hx) conditions. DAPT (1 μM) was added to inhibit Notch signaling. **(A)** Growth profiles of hADMPCs under Nx (red) and Hx (blue) conditions. Solid lines represent control cells and dotted lines represent DAPT-treated cells. The number of population doublings was calculated based on the total cell number at each passage. **(B)** Percentages of apoptotic cells with sub-G1 DNA. Results are presented as the mean of 3 independent experiments ± SD. **(C-D)** hADMPCs at passage 8 were induced for 3 weeks to differentiate into adipocytes **(C)** and osteoblasts **(D)** and stained with Oil Red O and Alizarin Red, respectively. The stained dye was extracted, and OD values were measured and plotted as the means of 3 independent experiments ± SD. **(E)** hADMPCs at passage 8 were induced for 3 weeks to differentiate into chondrocytes, and an immunofluorescent analysis of collagen II (red) was performed. The blue signals indicate nuclear staining. **(F)** hADMPCs were stained with SA-β-gal. \*P < 0.05 and \*\*P < 0.01 indicate significant difference (independent *t*-test) between Nx and Hx. Scale bars; 100 μm.

**Figure 6. Glycolysis is enhanced under 5% oxygen through Notch signaling. (A-D)** hADMPCs were expanded under normoxic (20% O<sub>2</sub>) and hypoxic (5% O<sub>2</sub>) conditions. DAPT (1 μM) was added in to inhibit Notch signaling. **(A)** Glucose consumption and lactate production of hADMPCs were measured and plotted as the means of 3 independent experiments ± SD. **(B)** Relative mRNA expression of *SLC2A3*, *TPI*, *PGK1*, *TIGAR*, and *SCO2* in hADMPCs. Each expression value was calculated with the  $\Delta\Delta C_t$  method using *UBE2D2* as an internal control. **(C, D)** Hexokinase (HK), phosphofructokinase (PFK), lactate dehydrogenase (LDH) **(C)**, pyruvate dehydrogenase (PDH), and Complex IV (Cox IV) **(D)** activities were measured and the value of relative activity was plotted as the means of 3 independent experiments ± SD. **(E, F)** hADMPCs were transduced with either mock (Cont) or HES1 and then cultured for 3 days. **(E)** Relative mRNA expression of *SLC2A3*, *TPI*, *PGK1*, *TIGAR*, and *SCO2* in hADMPCs. Each expression value was calculated with the  $\Delta\Delta C_t$  method using *UBE2D2* as an internal control. **(F)** Glucose consumption and lactate production of hADMPCs were measured and plotted as the means of 3 independent experiments ± SD. **(G)** hADMPCs were transduced with either scrambled control RNAi (Cont) or RNAi against HES1 (HES1-KD), and then cultured for 3 days. Glucose consumption and lactate production of hADMPCs were measured and plotted as the means of 3 independent experiments ± SD. \*\*P < 0.01. \* 0.01 < P < 0.05.

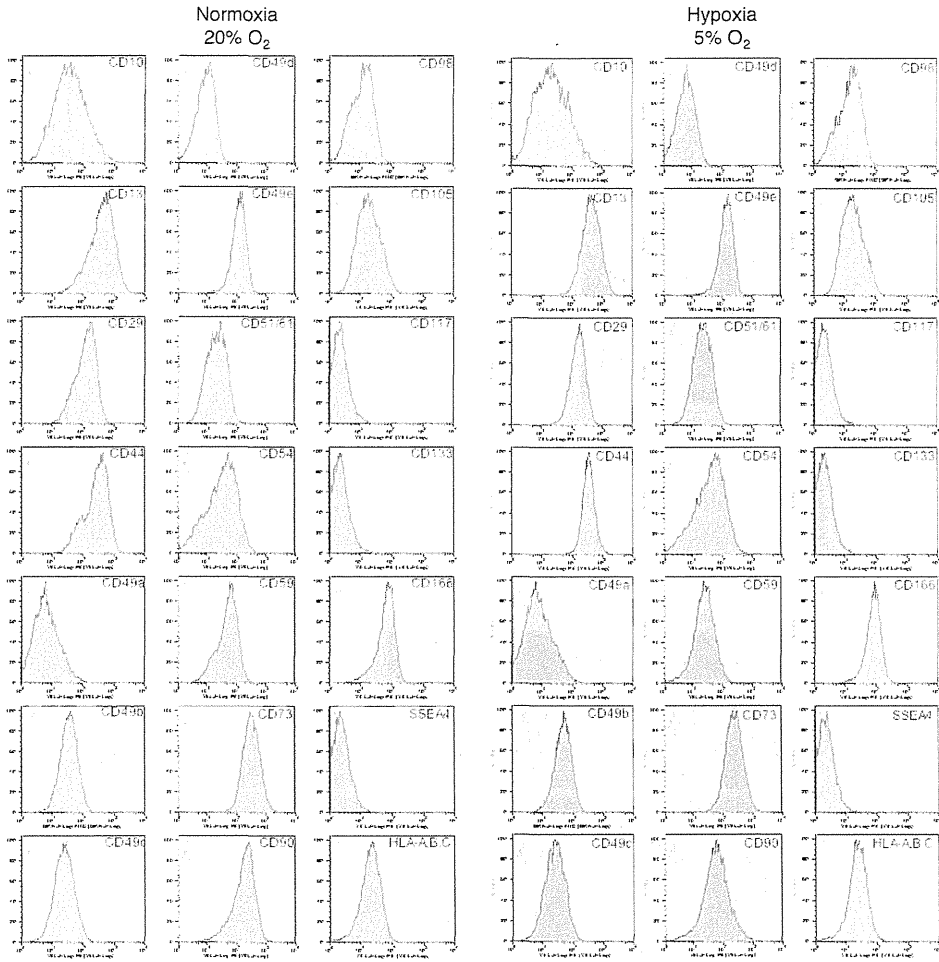
**Figure 7. Glycolysis supports proliferation of hADMPCs.** hADMPCs were treated with 0, 0.2, 0.4 and 1 mM 2-deoxy-D-glucose (2-DG) **(A)** or 0, 1 and 5 mM sodium azide (NaN<sub>3</sub>) **(B)** for 24 h. Cells were then allowed to

incorporate EdU for 2 h, and the EdU-positive cells were analyzed by flow cytometry. The percentages for the 0 mM control were plotted as the means of 3 independent experiments  $\pm$  SD. \*\*  $P < 0.01$ . \*  $0.01 < P < 0.05$ .



MoriyamaFig1  
170x237mm (300 x 300 DPI)

1  
2  
3  
4  
5  
6  
7  
8  
9  
10  
11  
12  
13  
14  
15  
16  
17  
18  
19  
20  
21  
22  
23  
24  
25  
26  
27  
28  
29  
30  
31  
32  
33  
34  
35  
36  
37  
38  
39  
40  
41  
42  
43  
44  
45  
46  
47  
48  
49  
50  
51  
52  
53  
54  
55  
56  
57  
58  
59  
60



MoriyamaFig2  
169x174mm (300 x 300 DPI)

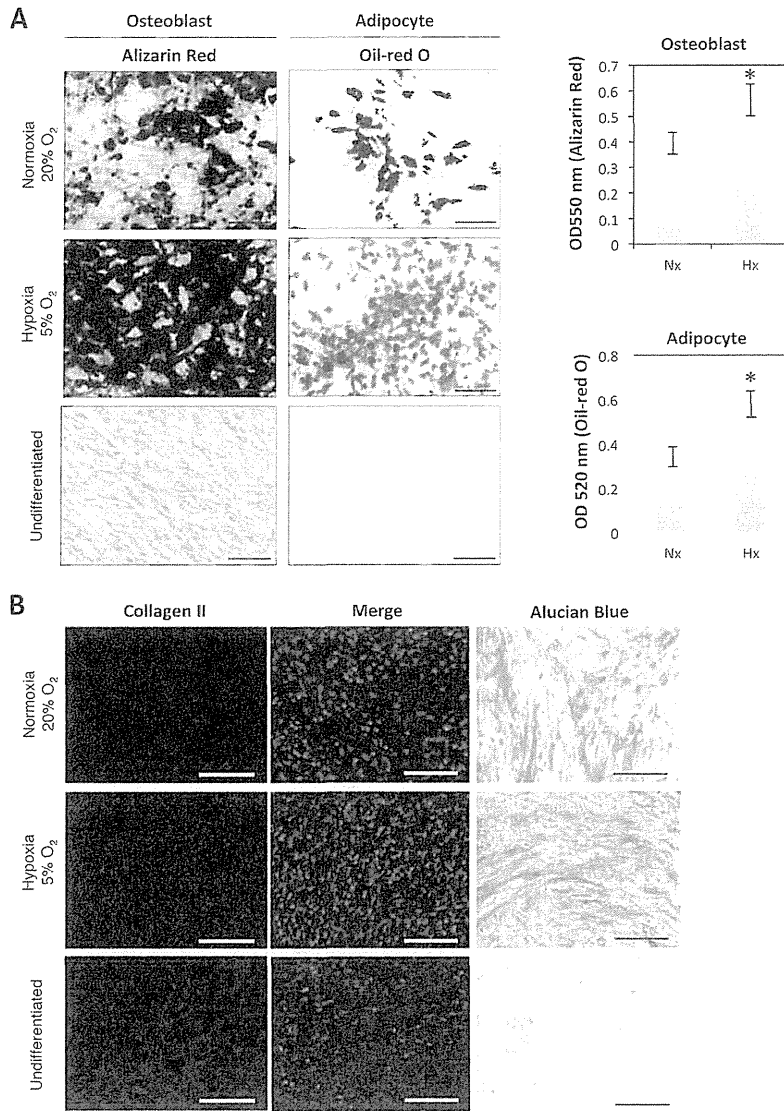
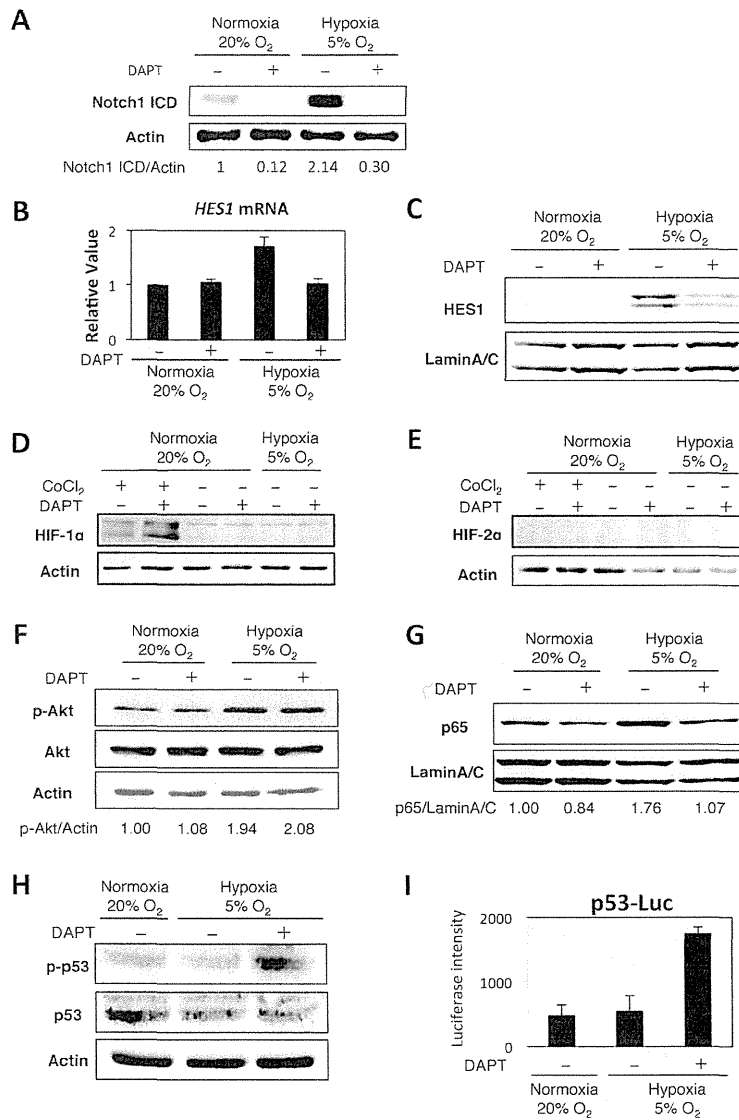


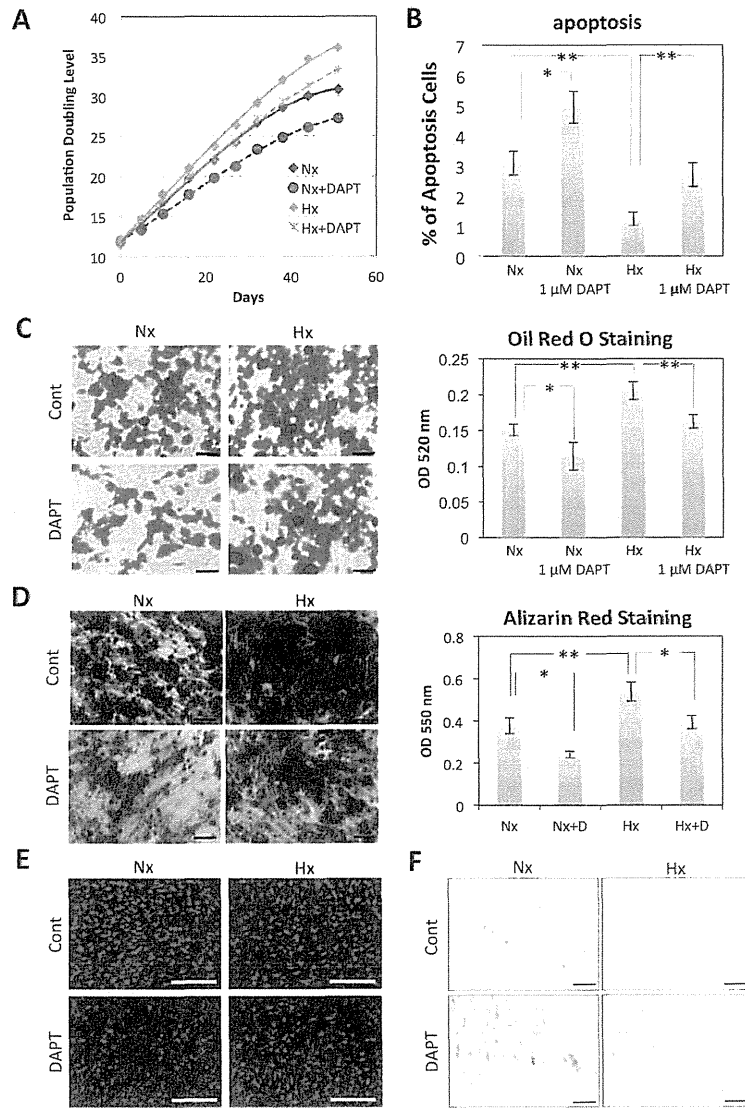
Figure 3  
101x144mm (300 x 300 DPI)



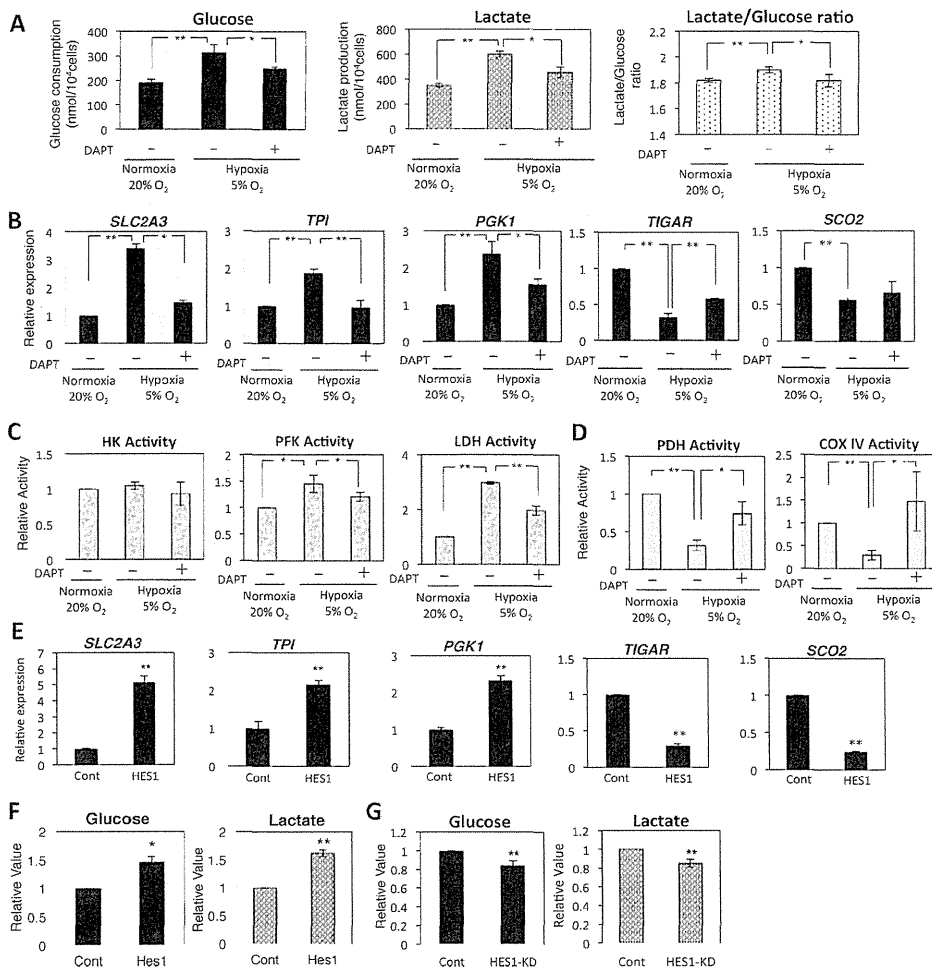
1  
2  
3  
4  
5  
6  
7  
8  
9  
10  
11  
12  
13  
14  
15  
16  
17  
18  
19  
20  
21  
22  
23  
24  
25  
26  
27  
28  
29  
30  
31  
32  
33  
34  
35  
36  
37  
38  
39  
40  
41  
42  
43  
44  
45  
46  
47  
48  
49  
50  
51  
52  
53  
54  
55  
56  
57  
58  
59  
60



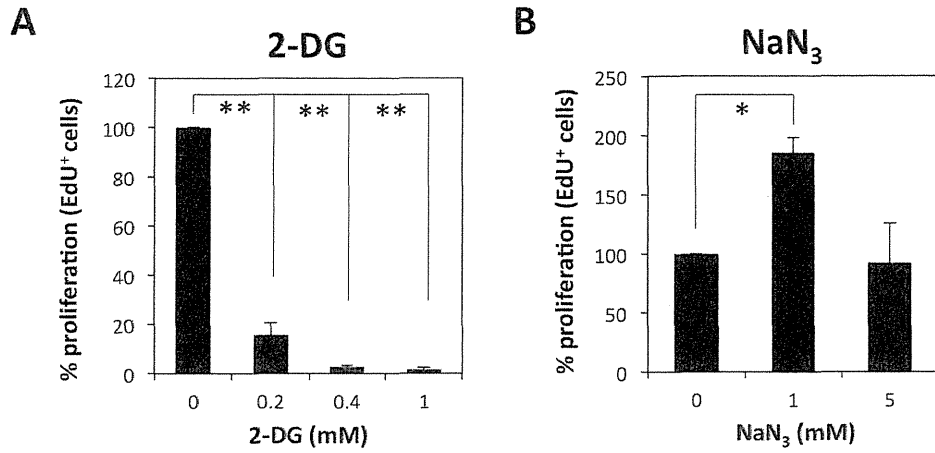
MoriyamaFig4  
163x246mm (300 x 300 DPI)



MoriyamaFig5  
171x247mm (300 x 300 DPI)



MoriyamaFig6  
169x176mm (300 x 300 DPI)



MoriyamaFig7  
151x72mm (300 x 300 DPI)